Cellular/Molecular

5-HT_{3A} Receptor-Bearing White Matter Interstitial GABAergic Interneurons Are Functionally Integrated into Cortical and Subcortical Networks

Jakob von Engelhardt, Sergey Khrulev, Marina Eliava, Sarah Wahlster, and Hannah Monyer
Department of Clinical Neurobiology, University Hospital Heidelberg and German Cancer Research Center (DKFZ), 69120 Heidelberg, Germany

In addition to axons and surrounding glial cells, the corpus callosum also contains interstitial neurons that constitute a heterogeneous cell population. There is growing anatomical evidence that white matter interstitial cells (WMICs) comprise GABAergic interneurons, but so far there is little functional evidence regarding their connectivity. The scarcity of these cells has hampered electrophysiological studies. We overcame this hindrance by taking recourse to transgenic mice in which distinct WMICs expressed enhanced green fluorescence protein (EGFP). The neuronal phenotype of the EGFP-labeled WMICs was confirmed by their NeuN positivity. The GABAergic phenotype could be established based on vasoactive intestinal peptide and calretinin expression and was further supported by a firing pattern typical for interneurons. Axons and dendrites of many EGFP-labeled WMICs extended to the cortex, hippocampus, and striatum. Patch-clamp recordings in acute slices showed that they receive excitatory and inhibitory input from cortical and subcortical structures. Moreover, paired recordings revealed that EGFP-labeled WMICs inhibit principal cells of the adjacent cortex, thus providing unequivocal functional evidence for their GABAergic phenotype and demonstrating that they are functionally integrated into neuronal networks.

Introduction

A century ago Ramon y Cajal (1911) described a class of neurons that are interspersed among the "white matter" fiber tracts and named them "interstitial cells" (WMICs) (Ramon y Cajal, 1911). Basic morphological features of WMICs were indicative of a neuronal phenotype (Neuburger, 1922; Lund et al., 1975; Kostovic and Rakic, 1980; Chun and Shatz, 1989; Muller, 1994; Shering and Lowenstein, 1994; Eastwood and Harrison, 2005; Friedlander and Torres-Reveron, 2009; Loup et al., 2009), a notion that was also supported by electron microscopy data (Valverde and Facal-Valverde, 1988). While there is ample information about the immunohistochemical signature of WMICs, such as the expression of GABA and specific GABAergic interneuron markers (Innis et al., 1979; Adrian et al., 1983; Schmechel et al., 1984; Shults et al., 1984; Somogyi et al., 1984; Chan-Palay et al., 1985; Sandell, 1986; Yan et al., 1996; Bayraktar et al., 1997; Tao et al., 1999; Suárez-Solá et al., 2009), only a few studies focused on electrophysiological properties of WMICs (Clancy et al., 2001; Torres-Reveron and Friedlander, 2007; Friedlander and Torres-Reveron, 2009). The main hindrance for the identification of WMICs in acute slices is their scarcity. We identified distinct WMICs by taking recourse to transgenic mice in which 5-HT_{3A} receptor-bearing interneurons express enhanced green fluorescence protein (EGFP) (Inta et al., 2008). These mice were originally generated to identify a subgroup of forebrain GABAergic interneurons that feature the expression of the ionotropic serotonin receptor type 5-HT_{3A} receptors (Tecott et al., 1993; Morales and Bloom, 1997). In addition to the labeling of forebrain interneurons in the gray matter (cortex, hippocampus, etc.), EGFP was also expressed in postnatally generated neurons derived from the subventricular zone. Furthermore and pertinent for this study, we detected in mature-appearing WMICs EGFP expression that enabled functional studies in acute slices. We performed anatomical and electrophysiological experiments of 5-HT_{3A}-EGFP-positive WMICs. Immunohistochemical experiments indicated that these cells are interneurons. WMICs are integrated into neuronal networks receiving excitatory and inhibitory input from cortical and subcortical regions and sending their axons to lower cortical layers. Paired recordings showed that EGFP-positive WMICs are inhibitory neurons targeting cortical principal cells.

Received Jan. 19, 2011; revised Aug. 19, 2011; accepted Aug. 24, 2011.

Author contributions: J.v.E. and H.M. designed research; J.v.E., S.K., M.E., and S.W. performed research; J.v.E. analyzed data; J.v.E. and H.M. wrote the paper.

This work was supported by the Schilling Foundation (to H.M.).

Correspondence should be addressed to Hannah Monyer at the above address. E-mail: monyer@dkfz.de.

DOI:10.1523/JNEUROSCI.0310-11.2011

 0270-6474/11/3116844-11$15.00/0

Materials and Methods

Immunohistochemistry. Immunohistochemical studies were carried out on 50 μm free-floating sections obtained from perfused brains of 5-HT_{3A}-EGFP mice (4% paraformaldehyde/0.1 M PBS, pH 7.4). EGFP-positive WMIC numbers were quantified by counting fluorescent cells in coronal slices of postnatal day (P)10 and adult mice (7–8 sections per mouse, 4 mice for each age). The following primary antibodies were used: rabbit anti-GFP, 1:5000 (Invitrogen); chicken anti-GFP, 1:3000 (Invitrogen); mouse anti-GAD67, 1:500 (Millipore), rabbit anti-calbindin, 1:3000 (Swant); mouse anti-calretinin, 1:5000 (Swant); mouse anti-parvalbumin, 1:3000 (Sigma-Aldrich); rat anti-somatostatin, 1:1000 (Millipore Bioscience Research Reagents); rabbit anti-VIP, 1:2000 (Immunostar); rabbit anti-neuropeptide Y (NPY), 1:2000 (Immunostar); mouse anti-tyrosine hydroxylase, 1:1000 (Sigma-Aldrich); mouse anti-

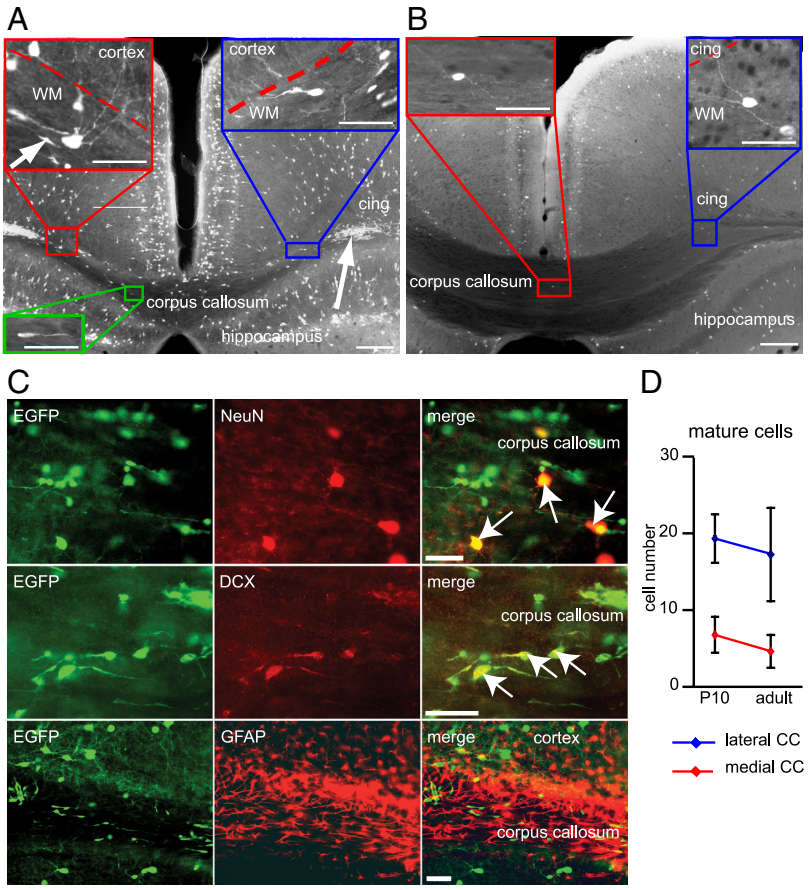

Figure 1. Mature and immature 5-HT_{3A}-EGFP-positive neurons are present in the white matter. ***A***, ***B***, 5-HT_{3A}-EGFP-positive neurons were abundant in the cortex and hippocampus of P10 (***A***) and adult (***B***) mouse brain (coronal sections). EGFP expression was furthermore detected in neurons with mature morphology (blue and red rectangle) in the subcortical white matter. In young mice, EGFP-labeled cells also comprised neuroblasts in the lateral (arrow) and medial (green rectangle) corpus callosum. These cells were scarce in the mature brain. Scale bars: overview, 200 μm; insets,50 μm. cing, Cingulum; WM, white matter. ***C***, Consistent with their morphology, mature-appearing EGFP-positive WMICs coexpressed NeuN while immature cells expressed doublecortin (DCX). There was no coexpression with the glial marker GFAP. Scale bar, 50 μm. ***D***, The number of EGFP-positive WMICs with mature morphology per coronal slice (50 μm) did not significantly change between P10 and adulthood (mean ± SD).

neuronal nitric oxide synthase (nNOS) 1:500 (Santa Cruz Biotechnology); mouse anti-neuronal nuclei (NeuN) 1:1000 (Millipore Bioscience Research Reagents); goat anti-doublecortin, 1:1000 (Santa Cruz Biotechnology); rabbit anti-M_2 muscarinic receptor, 1:500 (Alomone Labs); and mouse anti-glial fibrillary acidic protein (GFAP) 1:500. For visualization of primary antibodies, slices were incubated with the following secondary antibodies: goat anti-rabbit Alexa Fluor 488, 1:1000 (Invitrogen); goat anti-chicken Alexa Fluor 488, 1:1000 (Invitrogen); donkey anti-rabbit Alexa Fluor 488, 1:1000 (Invitrogen); goat anti-mouse Cy-3, 1:1000 (Jackson ImmunoResearch Laboratories); goat anti-rabbit Cy3, 1:1000 (Jackson ImmunoResearch Laboratories), donkey anti-goat Cy3, 1:500 (Jackson ImmunoResearch Laboratories); goat anti-mouse Cy5, 1:500 (Jackson ImmunoResearch Laboratories); and goat anti-rabbit Cy5 1:500 (Jackson ImmunoResearch Laboratories). Sections were analyzed using a confocal laser scanning microscope (LSM 5 Pascal, Zeiss) or a bright-field illumination fluorescent microscope (BX51W, Olympus).

Electrophysiology. Two hundred-micrometer-thick transverse slices were prepared from brains of P16–P30 transgenic mice. Slices were continuously superfused with ACSF (22−24°C or 34°C) containing the following (in mM): 125 NaCl, 2.5 KCl, 2 $CaCl_2$, 1 $MgCl_2$, 1.25 NaH_2PO_4, 25 $NaHCO_3$, and 25 glucose (pH 7.2, maintained by continuous bubbling with carbogen). Whole-cell recordings in current and voltage-clamp mode (no liquid junction potential correction) were performed using pipettes with a resistance of 5–7 MΩ when filled with the following (in mM): 105 K gluconate, 30 KCl, 4 Mg-ATP, 10 phosphocreatine, 0.3 GTP, and 10 HEPES, adjusted to pH 7.3 with KOH. $GABA_A$ receptors were blocked with 10 μM SR95531 hydrobromide (gabazine, Biotrend), AMPA receptors with 10 μM 6-cyano-7-nitroquinoxaline-2,3-dione (CNQX, Biotrend), and NMDA receptors with 50 μM D-APV (Biotrend). EPSCs and IPSCs were evoked by stimulating axons extracellularly with a glass pipette filled with ACSF. 5-HT_3 receptor-mediated currents and nicotinic acetylcholine receptor (nAChR)-mediated currents were elicited by pressure application of 100 μM serotonin (in ASCF) and 100 μM carbamylcholine chloride (carbachol, Sigma-Aldrich), respectively, onto EGFP-positive WMICs via a glass pipette. During 5-HT_3 receptor-mediated and nAChR-mediated current recordings $GABA_A$, AMPA, and NMDA receptors were blocked with 10 μM gabazine, 10 μM CNQX, and 50 μM D-APV, respectively. Nicotinic acetylcholine receptor (nAChR)-mediated currents were recorded in the presence of the muscarinic AChR antagonist atropine (10 μM, Sigma-Aldrich). nAChR-mediated currents were blocked by 10 μM dihydro-β-erythoidine hydrobromide (DHβE; Tocris Bioscience). EGFP-positive neurons were visually identified using an upright microscope (BX 51, Olympus) equipped with infrared-differential interference contrast (DIC) and standard epifluorescence. Stimulus delivery and data acquisition was performed using Patchmaster software (Heka Elektronik). Signals were filtered at 1–3 kHz and sampled at 10 kHz, and off-line analysis was performed using Igor Pro (Wavemetrics).

Electrophysiological analysis. The analysis of electrophysiological properties was performed essentially as described previously (von Engelhardt et al., 2007). Hyperpolarizing and depolarizing current pulses (1 s) were applied to calculate input resistance and threshold potential. Action potential (AP) waveforms were analyzed at just suprathreshold potential. The AP and afterhyperpolarization (AHP) amplitude was measured from threshold to peak of the AP or AHP. The duration of the AP was measured at half-amplitude. f_{burst}, f_{200}, and f_{last} (all in Hz) were measured at the submaximal current step applied before spike inactivation became evident and were calculated from the reciprocal of the first interspike interval (ISI), the ISI after 200 ms, and the last ISI, respectively. The early and late frequency adaptation (percentage) was calculated according to $[100 \times (f_{burst} - f_{200})/f_{burst}]$ and $[100\times (f_{200} - f_{last})/f_{200}]$, respectively. Firing patterns were subclassified into nonadapting (late adaptation, ≤20%; early adaptation, ≤40%), nonadapting with an initial burst (late adaptation, ≤20%; early adaptation, ≥40%), adapting (late adaptation, ≥21%; early adaptation, ≤70%), adapting firing pattern with an initial burst (late adaptation, ≥21%; early adaptation, ≥70%), and irregular firing pattern. Conduction velocity of axons that innervate EGFP-positive neurons and synaptic delay were estimated by recording EPSC delays (from start of stimulus artifact to start of EPSC) at 34°C and at 22°C and plotting them against the distance of the stimulation pipette to the cell. A linear fit of these data was used to obtain conduction velocity (slope) and synaptic delay (x-intercept).

Development of biocytin-filled cells. Brain slices of P16–P30 mice were prepared as described for electrophysiology. Neurons were patch clamped for 10–30 min with biocytin in the pipette. For filling of connected pairs, EGFP-expressing cells in the corpus callosum were immediately patched with biocytin in the pipette and cortical cells were patched clamped with normal intracellular solution. After finding a con-

nected pair, the cortical neuron was repatched with biocytin in the intracellular solution. After the pipette was withdrawn, slices were kept in the recording chamber for additional 10 min and immersion fixed in 4% paraformaldehyde/0.1 M PBS for 8–16 h at 4°C. Biocytin-filled cells were incubated with peroxidase-avidin-biotin complex (ABC, Vector Laboratories) and visualized with DAB-nickel sulfate. Subsequently, slices were mounted onto microscope slides and coverslipped with Mowiol. The biocytin-filled neuron reconstruction was performed with the aid of a Neurolucida 3D reconstruction system and NeuroExplorer Software package MicroBrightField and NeuroExplorer).

Statistics. Data are presented as mean ± SD or SEM, as indicated. Statistical analyses were performed using SigmaStat 3.11. Differences between groups were examined using Student's *t* test, one-way ANOVA with Bonferroni *t* test for multiple-comparisons, Mann–Whitney rank sum test, or Kruskall–Wallis one-way ANOVA with a Dunn's post-test for multiple comparisons as indicated. Normality of data distribution was tested by Kolmogorov–Smirnov test and equal variance by Levene median test. Values of $p < 0.05$ were considered statistically significant.

Results

5-HT$_{3A}$ receptor BAC transgenic mice express EGFP in mature WMICs

In 5-HT$_{3A}$-EGFP mice the expression of the fluorescent protein was detected in a subset of mature GABAergic interneurons and in postnatally generated neurons derived from the subventricular zone (Inta et al., 2008). The latter eventually populate the olfactory bulb and the cortex. It was hence not surprising to find in slices from transgenic mice EGFP-labeled immature neurons traversing the corpus callosum (Fig. 1*A*,*B*). These cells were positive for doublecortin (Fig. 1*C*), a marker for immature and migrating cells. We performed time-lapse imaging experiments over several hours using acute coronal slices to provide direct evidence of the migratory phenotype for white matter cells with immature morphology (data not shown). However, EGFP expression within the corpus callosum was not restricted to these small neuroblasts but was also detected in larger neurons (somata with 20–30 μm longitudinal axis) with elaborate dendritic and axonal arborization typical for mature cells (Fig. 1 *A*,*B*). Most large EGFP-positive cells expressed NeuN (94.72 ± 6.94%), a marker for mature neurons, and were doublecortin negative. Approximately a third of all NeuN-positive white matter cells expressed EGFP (P10, 35.35 ± 5.21%; adult, 26.31 ± 7.5%). EGFP-positive WMICs did not colocalize with the astrocytic marker GFAP (Fig. 1*C*). We quantified the absolute number of mature EGFP-positive neurons that were more numerous in the lateral than in the medial part of the corpus callosum. There was no significant age-dependent decline in the number of EGFP-positive WMICs between P10 and adult mice (Fig. 1*D*).

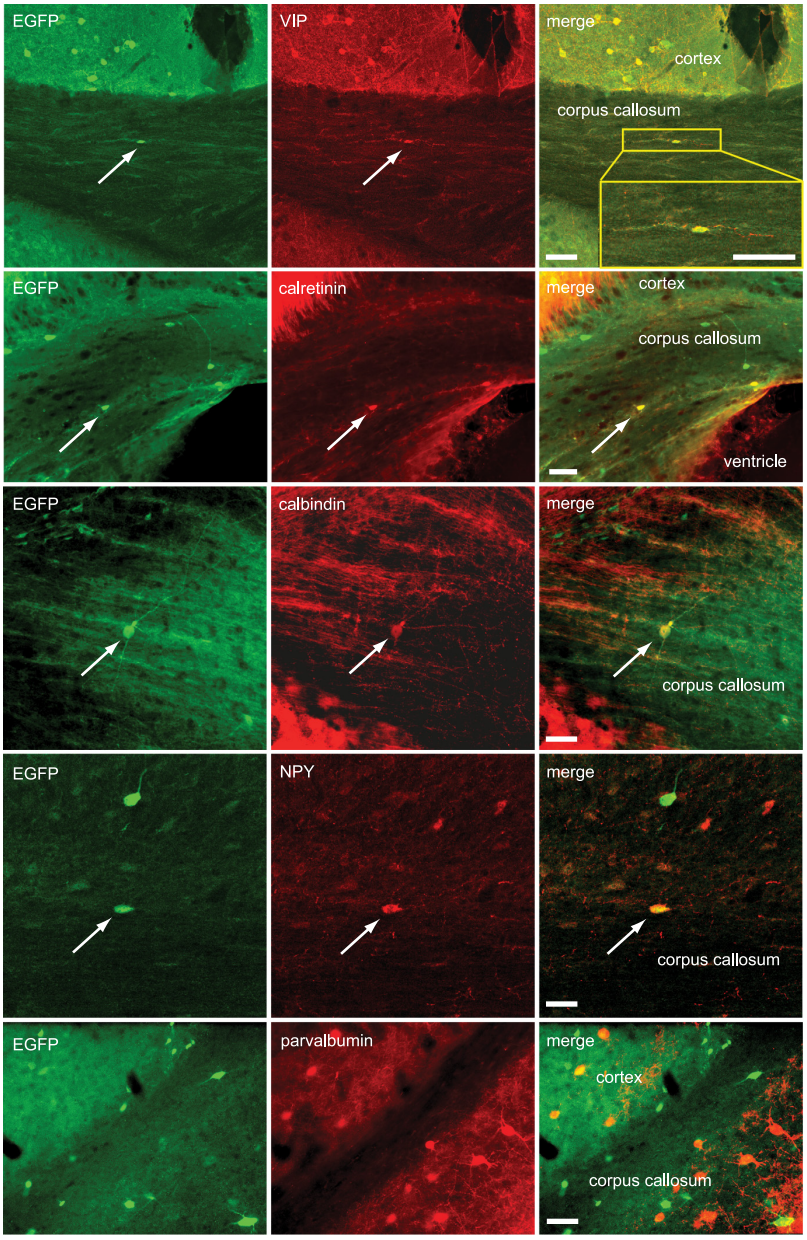

Figure 2. EGFP-positive WMICs express GABAergic interneuron markers. Double-labeling immunohistochemistry with antibodies against EGFP and VIP, calretinin, calbindin, NPY, and parvalbumin. Arrows point to EGFP-positive cells that coexpressed the indicated interneuron marker. EGFP and parvalbumin did not colocalize in WMICs. Scale bars, 50 μm.

EGFP-positive WMICs coexpress different interneuron markers

As 5-HT$_{3A}$ receptor expression is confined to interneurons, we investigated the coexpression of EGFP and a series of interneuronal marker proteins in corpus callosum neurons. The highest overlap was found for the interneuron markers VIP and calretinin. All VIP-positive and most calretinin-positive cells expressed EGFP in young (P10) and adult mice. Approximately a third of EGFP-positive cells expressed VIP and calretinin, respectively (Fig. 2). Other interneuron markers (calbindin, NPY, somatostatin) were less frequently expressed in EGFP-positive cells and, conversely, only some of these cells expressed EGFP (Table 1, Fig. 2). We also detected nNOS-, tyrosine hydroxylase-, and M_2 muscarinic receptor-positive cells in the corpus callosum, as reported previously (Mizukawa et al., 1988; Smiley et al., 1999; Tao et al., 1999; Raghanti et al., 2009; Suárez-Solá et al., 2009), but none of them ex-

Table 1. Co-expression of EGFP and interneuron marker proteins

	Percentage of marker-expressing cells coexpressing EGFP (%)		Percentage of EGFP-expressing cells coexpressing IN markers (%)	
	P10	Adult	P10	Adult
VIP	100	100	26.5 ± 13.1	30.4 ± 7.6
Calretinin	72 ± 25	88 ± 14.8	32.9 ± 16.4	19.6 ± 11.7
Calbindin	45.3 ± 6.9	34.9 ± 21.6	9.6 ± 4.2	8.4 ± 4.7
NPY	0	18.4 ± 8.5*	0	13.4 ± 4.1*
Somatostatin	0	7.95 ± 10.4*	0	2.7 ± 3.2*
Other markers #	0	0	0	0

#Tyrosine hydroxylase, M_2 muscarinic receptor, nNOS, parvalbumin. *$p < 0.05$ (P10 vs adult).

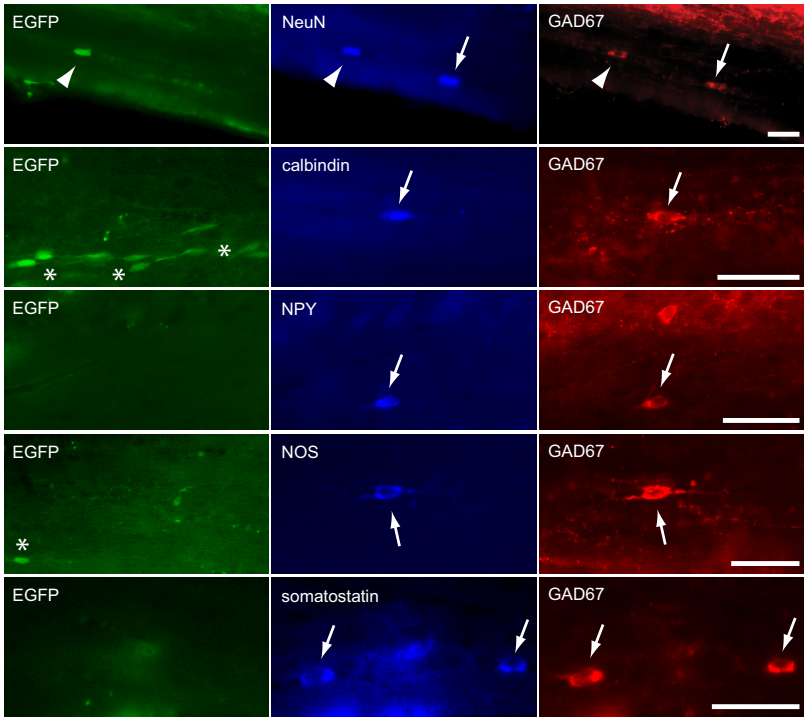

Figure 3. EGFP-negative GABAergic WMICs comprise different interneuron subtypes. Arrows point to GAD67-positive/EGFP-negative WMICs that were positive for NeuN, calbindin, NPY, NOS, and somatostatin, respectively. The arrowhead indicates a NeuN/GAD67-positive cell that was EGFP positive. Asterisks point to immature EGFP-positive GAD67-negative cells. Immunohistochemistry was performed with antibodies against NeuN, GAD67 calbindin, NPY, NOS, and somatostatin. Scale bars, 50 μm.

pressed EGFP. No parvalbumin-positive cells were found in the corpus callosum (Fig. 2).

The double-labeling immunohistochemistry experiments indicated that not all GABAergic WMICs are 5-HT_{3A}-EGFP positive. Indeed, immunohistochemical experiments revealed that only 58% of NeuN/GAD67-positive cells expressed EGFP (Fig. 3). The remaining EGFP-negative GAD67-positive WMICs expressed NPY, calbindin, somatostatin and nNOS (Fig. 3).

EGFP-positive WMICs exhibit distinct morphological and electrophysiological properties

To study morphological and electrophysiological properties of EGFP-positive WMICs, we performed whole-cell patch-clamp experiments. EGFP-labeled cells could readily be identified in acute coronal brain slices of juvenile brains (from bregma 1.1 to bregma −1.7) (Fig. 4*A*). We analyzed the anatomy of 53 biocytin-filled EGFP-positive WMICs (Fig. 4*B* and Table 2). EGFP-positive cell bodies were found mainly in the upper and middle third of the white matter (upper third, 38 cells; middle third, 11 cells; lower third, 4 cells). Most EGFP-positive WMICs had interneuron like morphologies with locally confined dendritic and axonal arbors. Three to five primary dendrites emerged from the soma. Dendrites were aspinous but often had irregular varicosities. Most EGFP-positive WMICs (35 cells, designated here as type 1) had medium size oval or fusiform perikarya that had horizontal, occasionally vertical orientations and were located in the upper third of the lateral corpus callosum and subcortical white matter. They usually extended their processes to lower layers of the overlying cortex. Some EGFP-positive WMICs (15 cells, designated as type 2) had small and round somata, located in the middle and lower third of the medial part of the corpus callosum, and processes that were usually confined to the white matter. The beaded axon-like processes of these cells were thin (in some cases not clearly distinguishable), and the axon of six cells crossed the midline, arborizing in the contralateral corpus callosum and cingulum.

Strikingly, in a few cases WMICs were anatomically not classical "interneurons" since they connected different brain areas (e.g., see Fig. 5*A*,*B*, showing a cell with dendrites in the striatum and its axon in the cortex, and Fig. 6, showing a cell with dendrites in the cortex and hippocampus and the axon in the cortex).

Basic electrophysiological properties of EGFP-positive WMICs are summarized in Table 3 (age of mice, P29 ± 0.7). All cells had a typical interneuron firing pattern. Five firing pattern types could be distinguished (see Materials and Methods for further details regarding the subclassification): The majority of cells (63%) had a nonadapting firing pattern either with (45%, Fig. 4*A*) or without (18%) an initial burst of action potentials. Fifteen percent of the neurons fired irregularly. The rest of the neurons exhibited an adapting firing pattern with (13%) or without (10%) an initial burst of action potentials. In 53% of the cells a first and fast AHP was followed by a short depolarization and a subsequent slower second AHP that together formed a characteristic triphasic waveform (Fig. 4*A*). Most passive and active electrophysiological properties (Table 3) were alike in interneurons with different firing patterns (excluding early and late adaptations that were used for classification). Only the input resistance, the AHP, and the maximal firing frequency were significantly different between cell types with different firing patterns (Table 3). We compared electrophysiological properties of WMICs of P29 mice with those of neurons of P17 (± 0.5) mice. We observed significant differences in threshold potential (P17: 38.5 [36–40] mV, $n = 60$; P29: 41 [39–44] mV, $n = 40$; median [interquartile range (IQR)], $p < 0.00001$, Mann–Whitney test), action potential duration (P17: 0.57 [0.5–0.66] ms, $n = 60$; P29: 0.51 [0.45–0.6] ms, $n = 40$; median [IQR], $p < 0.04$, Mann–Whitney test), and maximal frequency (P17: 51.9 ± 34 Hz, $n = 60$; P29: 81 ± 43 Hz, $n = 40$; mean ± SD, $p < 0.0002$, t test). These differences indicated that WMICs continue to mature between P17 and P29.

EGFP-positive corpus callosum interneurons receive GABAergic and glutamatergic input

Spontaneous EPSCs (sEPSCs) and IPSCs (sIPSCs) could be detected in all EGFP-positive WMICs (Fig. 4*C*). We performed recordings using a high intracellular Cl^--concentration that facilitates the analysis of GABAergic currents at resting membrane potential. There was no difference in sEPSC and sIPSC interevent intervals (IEIs) when compared to sEPSC and sIPSC IEIs of cortical EGFP-positive neurons (sEPSC IEI WMIC: 792 ms [366–3639], $n = 16$; sEPSC IEI cortical interneuron: 631 ms [334–1063], $n = 18$, $p > 0.05$; sIPSC IEI WMIC: 557 ms [340–3475], $n = 17$; sIPSC IEI cortical interneuron: 577 ms [440–1993], $n = 15$, $p > 0.05$; median [IQR]). sEPSC amplitude, rise time, and decay time constant were comparable in WMICs and cortical EGFP-positive cells (sEPSC amplitude WMIC: -16.5 ± 6.7 pA, $n = 16$; sEPSC amplitude cortical interneuron: -14.6 ± 3.6 pA, $n = 18$, $p > 0.05$; sEPSC rise time WMIC: 0.52 ± 0.13 ms, $n = 16$; sEPSC rise time cortical interneuron: 0.55 ± 0.11 ms, $n = 18$, $p > 0.05$; sEPSC decay time constant WMIC: 2.9 ± 1 ms, $n = 16$; sEPSC decay time constant cortical interneuron: 2.8 ± 0.9 ms, $n = 18$, mean $\pm$ SD, $p > 0.05$). There was also no difference in sIPSC rise time and decay time constant, but sIPSC amplitudes were significantly bigger in WMICs than in cortical EGFP-positive cells (sIPSC amplitude WMIC: -18.7 ± 6.2 pA, $n = 17$; sIPSC amplitude cortical interneuron: -13.6 ± 3.6 pA, $n = 15$, $p < 0.05$; sIPSC rise time WMIC: 0.46 ± 0.25 ms, $n = 17$; sIPSC rise time cortical interneuron: 0.53 ± 0.34 ms, $n = 15$, $p > 0.05$; sIPSC decay time constant WMIC: 5.3 ± 1.4 ms, $n = 17$; sIPSC decay time constant cortical interneuron: 4.7 ± 1.2 ms, $n = 15$, mean $\pm$ SD, $p > 0.05$, *t* test).

No spontaneous postsynaptic currents were recorded when GABAergic and glutamatergic currents were blocked simultaneously, indicating that other ionotropic receptors do not contribute considerably to the activation or inhibition of EGFP-positive neurons in the corpus callosum. This was surprising, given that in these transgenic mice EGFP expression is driven by the 5-HT_{3A}-receptor promoter. It is possible that the release probability of serotonin-containing vesicles is very low and/or that innervation via serotonergic fibers is scarce, making the occurrence of spontaneous 5-HT_3 receptor-mediated EPSCs unlikely even during prolonged recordings. Also upon extracellular stimulation in

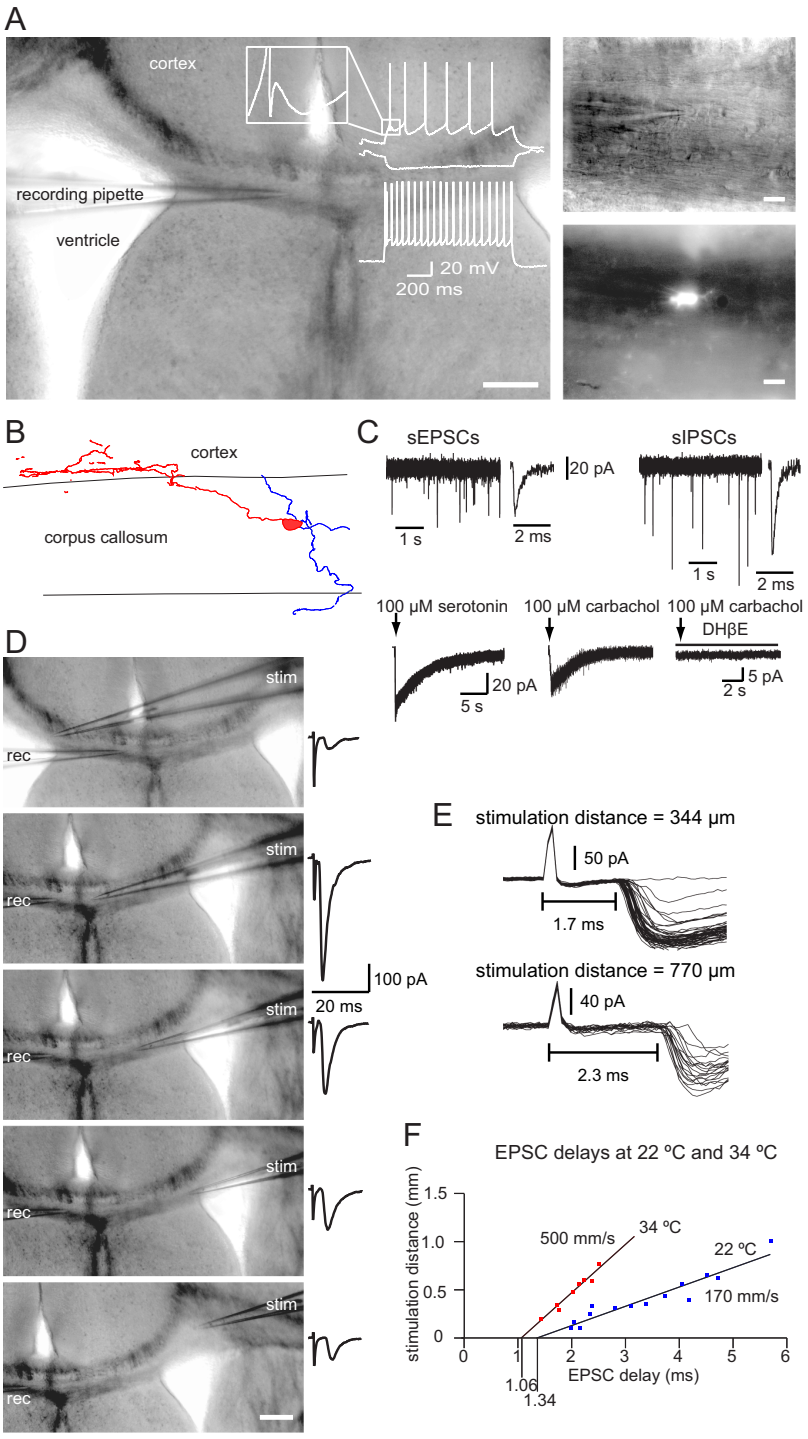

Figure 4. EGFP-positive WMICs show electrophysiological properties typical for mature neurons. ***A***, The DIC image of the acute slice illustrates location of the recording pipette (left) and the higher-magnification images on the right show a WMIC in the corpus callosum and the EGFP signal of the cell. Scale bars: Left, 200 μm; right, 20 μm. The cell responded to hyperpolarizing and depolarizing current injections with a nonadapting firing pattern and an initial burst of two action potentials at higher current injections. The inset illustrates the characteristic triphasic AHP waveform. ***B***, Reconstruction of a representative biocytin-filled WMIC with dendrites (blue) confined to the corpus callosum and the axon (red) arborizing in lower cortical layers. ***C***, Example traces of sEPSC and sIPSC recordings (top traces). Pressure application of 100 μM serotonin elicited 5-HT_3 receptor-mediated currents in an EGFP-positive WMIC (bottom trace, left). Pressure application of 100 μM carbachol elicited nAChR-mediated currents in an EGFP-positive WMIC. This current was blocked by DHβE (bottom traces, right). ***D***, DIC images with a stimulation pipette (stim) at different locations. Scale bar, 200 μm. Stimulation within the ipsilateral (top image) and contralateral (bottom four images) sides of the corpus callosum elicited EPSCs in the EGFP-positive WMIC. Part of the stimulus artifact is truncated. rec, Recording. ***E***, Repeatedly evoked EPSCs with the stimulation pipette located at a distance of 344 μm (top traces) and 770 μm (bottom, traces) from the recorded cell. ***F***, EPSC delays increased linearly with the distance of the stimulation pipette to the cell at 22°C and 34°C. The calculated conduction velocities were consistent with an activation of WMICs via nonmyelinated axons.

Table 2. Neurite location of WMICs

	Confined to white matter	Projecting to cortex	Projecting to other structures
Dendrites	$n = 22$	$n = 25$	2 (hippocampus), 4 (striatum)
Axon	$n = 20$	$n = 25$	1 (hippocampus)

Axons of seven cells were truncated. n = number of cells with their processes in the indicated areas.

the corpus callosum, cortex, or striatum, no 5-HT_3 receptor-mediated currents could be evoked in EGFP-positive WMICs. However, pressure-application of serotonin (100 μM) via a glass pipette evoked 5-HT_3 receptor-mediated currents with a mean amplitude of 61 ± 28.7 pA in 8 of 9 EGFP-positive WMICs (Fig. 4*C*). Similarly, pressure application of carbachol (100 μM, + 10 μM atropine) elicited nAChR-mediated currents with a mean amplitude of 9.8 ± 8.1 pA in 14 of 15 EGFP-positive WMICs that was blocked by the nAChR antagonist DHβE (10 μM, 4 of 4 cells) (Fig. 4*C*).

To identify the source of glutamatergic inputs to EGFP-positive WMICs, we stimulated axons at different locations. EPSCs could be evoked readily by stimulating axons in the corpus callosum, the cortex, and the striatum (Fig. 5). Importantly, stimulation of axons in the ipsilateral and contralateral corpus callosum and cortex elicited EPSCs in EGFP-positive WMICs (Fig. 4*D*). The estimated axonal conduction velocity was 500 mm/s at 34°C and 170 mm/s at 22°C, consistent with an innervation of EGFP-positive WMICs via nonmyelinated axons. The synaptic delays were 1.06 and 1.34 ms at 34°C and 22°C, respectively (Fig. 4*E*,*F*). These measures are only an approximation, since an exact calculation would require stimulation of only one axon type and information regarding the axon length.

EGFP-positive corpus callosum interneurons inhibit cortical neurons

Reconstruction of biocytin-filled, EGFP-positive WMICs indicated that they innervate mainly neurons in lower cortical layers. To identify target neurons, we performed paired recordings of EGFP-positive cells and randomly selected lower layer cortical cells. Five of two hundred thirty pairs were synaptically connected. Since EGFP-positive neurons were most abundant in the middle part of the white matter (i.e., the corpus callosum), it was not surprising that the cells to which they were synaptically connected were neurons located in the cortical area above, namely in the cingulate and retrosplenial cortex.

In four connected pairs, the presynaptic cell was an EGFP-positive WMIC (firing pattern: 2× nonadapting with burst, 1× nonadapting, 1× adapting). In all four cases, the postsynaptic cell was located in the cingulate cortex. Upon depolarizing current injection, three of the four postsynaptic cells exhibited firing patterns typical for principal cells, and one revealed an interneuron-type firing pattern (nonadapting). After identification of a connected pair, we repatched the cortical neuron with biocytin in the pipette (the pipette for the WMICs always contained biocytin). Two of the four connected pairs were successfully reconstructed. One of the 2 postsynaptic neurons was a spiny pyramidal cell (Fig. 7*A*), the other a spiny stellate cell. Both cells were located in layer V of the cingulate cortex. The EGFP-positive neuron, presynaptic to the pyramidal cell, was located in the upper third of the corpus callosum and had an oval cell body with several aspiny and occasionally varicose dendrites confined to the corpus callosum. Its heavily beaded axon originated from a main dendrite (Fig. 6*B*,*C*) and formed an elaborate axonal plexus in the cingulate cortex overlapping with the apical dendrites of the postsynaptic pyramidal cell (Fig. 6*B*). We found three close appositions (putative synapses) between EGFP-positive WMIC axon boutons and pyramidal cell dendritic shafts (Fig. 7*D*–*F*). The EGFP-positive neuron, presynaptic to the spiny stellate cell, had both dendrites and the axon in the cingulate cortex, the latter overlapping with the spiny stellate cell dendrites.

Action potentials were evoked in EGFP-positive presynaptic cells by direct current injection, and IPSPs and IPSCs were recorded in the postsynaptic cell in current and voltage-clamp mode, respectively. The average IPSP amplitude was 7 ± 7.6 mV (± SD) and the IPSC amplitude 114 ± 14 pA (± SD). IPSPs and IPSCs exhibited paired-pulse depression [paired-pulse ratio (PPR) IPSP with 50 ms IEI: 0.78 ± 0.53; PPR IPSC with 50 ms IEI: 0.92 ± 0.03, mean ± SD, $n = 3$). Responses in the postsynaptic cell could be completely blocked by the $GABA_A$ receptor antagonist gabazine, consistent with the GABAergic phenotype of EGFP-positive corpus callosum interneurons (Fig. 7*G*).

One of the five connected pairs comprised a presynaptic lightly spinous pyramidal cell located in layer 6 of the retrosplenial cortex and a postsynaptic EGFP-positive corpus callosum interneuron (firing pattern: nonadapting with burst) (Fig. 8*A*,*B*). Both cells were successfully filled with biocytin and subsequently reconstructed. The presynaptic principal cell had a triangular shape with the basilar mildly spinous dendrites mainly in layer 6 of retrosplenial cortex. Only a short portion of the axon that was presumably cut during slicing procedure could be visualized in the upper layers of the retrosplenial cortex. The postsynaptic EGFP-positive cell was located in the upper third of the corpus callosum and had an oval soma with an axon running along the corpus callosum toward the contralateral hemisphere. Its dendritic arbor was located within the corpus callosum and extended into the adjacent cortex where some dendrites were in close proximity to the axon of the presynaptic cell (Fig. 8*D*). The average EPSPs amplitude recorded in the postsynaptic EGFP-positive WMIC was 0.8 mV, and paired EPSPs exhibited strong facilitation (PPR EPSPs with 50 ms IEI: 4.5) (Fig. 8*C*).

Discussion

In this study we used 5-HT_{3A}-EGFP mice to identify a distinct subpopulation of WMICs. Immunohistochemical, electrophysiological, and anatomical properties provided evidence that these cells are mature neurons that can be easily distinguished from EGFP-labeled migrating neuroblasts traversing the corpus callosum. Colocalization with classical interneuron markers and anatomical features such as lack of dendritic spines and firing pattern indicated that the EGFP-positive WMICs are GABAergic interneurons. The GABAergic phenotype of some 5-HT_{3A}-EGFP-positive WMICs was further demonstrated by paired recordings with EGFP-positive WMICs as presynaptic cells and cortical neurons as postsynaptic cells, since the postsynaptically recorded IPSCs and IPSPs could be blocked by a $GABA_A$ receptor antagonist. EGFP labeled 58% of NeuN/GAD67-positive cells, indicating that in this study we investigated only a subgroup of GABAergic WMICs.

Based on previous immunohistochemical studies analyzing the expression of different interneuron markers, it can be inferred that WMICs comprise heterogeneous interneuron populations. Thus, the presence of calretinin (Suárez-Solá et al., 2009), calbindin (Yan et al., 1996), VIP (Bayraktar et al., 1997, 2000), NPY (Adrian et al., 1983; Chan-Palay et al., 1985), cholecystokinin (Innis et al., 1979), substance P (Shults et al., 1984), somatostatin (Somogyi et al., 1984), and nNOS (Sandell, 1986; Tao et al., 1999; Suárez-Solá et al., 2009) was reported for WMICs. Of note, in the transgenic mice employed here, EGFP expression in the corpus callosum was confined by and large to VIP-,

Table 3. Electrophysiological properties of EGFP-positive WMICs

	Nonadapting with burst (1)	Nonadapting (2)	Adapting with burst (3)	Adapting (4)	Irregular (5)
Percentage (%) of all cells (*n*)	45 (18)	17.5 (7)	12.5 (5)	10 (4)	15 (6)
Input resistance (MΩ)	356 ± 220	602 ± 257* (vs 3)	224 ± 26	480±152	616 ± 223* (vs 3)
Membrane potential (mV)	69 ± 9	80 ± 8	69 ± 5	77 ± 12	81 ± 7
Threshold potential (mV)	41 ± 4	45 ± 5	41 ± 2	41 ± 1	42 ± 3
Sag (mV)	2.1 ± 2.2	1.5 ± 1	3.2 ± 2.2	0.7 ± 0.9	3 ± 3
Amplitude of 1 st AP (mV)	79 ± 12	86 ± 8	84 ± 11	78 ± 15	79 ± 18
Amplitude of 2 nd AP (mV)	77 ± 13	81 ± 6	80 ± 13	76 ± 15	76 ± 16
1 st AP half width (ms)	0.54 ± 0.14	0.51 ± 0.09	0.5 ± 0.06	0.5 ± 0.03	0.52 ± 0.11
2 nd AP half width (ms)	0.6 ± 0.15	0.6 ± 0.17	0.56 ± 0.07	0.51 ± 0.02	0.59 ± 0.14
Amplitude of 1 st AHP (mV)	13 ± 6* (vs NAC)	20 ± 4	11 ± 4* (vs 2)	20 ± 4* (vs 3)	18 ± 4
Amplitude of 2 nd AHP (mV)	15 ± 4*** (vs 2)	22 ± 2** (vs 3)	13 ± 2* (vs 4)	21 ± 4* (vs 1)	19 ± 2
Maximal frequency (Hz)	77.5 ± 35*	128 ± 51	75 ± 34	89 ± 20	39 ± 20** (vs 2)
Early adaptation (%)	70 ± 11*** (vs 2)	30 ± 7*** (vs 3)	77 ± 11*** (vs 4)	47 ± 5*** (vs 3)	
Late adaptation (%)	6.8 ± 9.5*** (vs 3)	11 ± 4* (vs 3)	24 ± 5	24 ± 5** (vs 2)	

*$p < 0.05$, **$p < 0.01$, ***$p < 0.001$.

calretinin-, and calbindin-positive interneurons. Many WMICs expressed nNOS, NPY, and somatostatin, consistent with previous studies, but only a few EGFP-expressing WMICs were positive for these markers.

Electrophysiological characterization indicated that EGFP-expressing WMICs were not a homogeneous cell group, as we distinguished five firing patterns that were previously reported for cortical interneurons (Kawaguchi and Kubota, 1996, 1997; Markram et al., 2004). EGFP-positive WMIC diversity was revealed also by the anatomical features of these neurons. Thus, the fluorescently labeled population comprised two cell groups, i.e., cells with dendrites and axons extending beyond the white matter boundaries with preferential arborization in lower cortical layers, but also in the hippocampus and striatum (type 1), and smaller cells located in the lower third of the corpus callosum with processes confined by and large to the white matter (type 2). WMICs with axons projecting to the cortex were described previously (Meyer et al., 1991; Clancy et al., 2001; Tomioka and Rockland, 2007). Most EGFP-positive WMICs had comparably small axonal arbors and do not meet the criteria of long-range GABAergic projection neurons with an axonal arbor extending >1.5 mm into the cortex (Tomioka et al., 2005). Previous studies reported the presence of long-range GABAergic projection neurons in the white matter. Most of these cells express nNOS, NPY, and somatostatin (Tomioka et al., 2005; Higo et al., 2007, 2009; Tomioka and Rockland, 2007; Tamamaki and Tomioka, 2010) and are not identical with the cell population characterized in this study. Interestingly, some EGFP-positive WMICs have dendrites in the striatum and hippocampus and axons reaching into the cortex. Hence, it is likely that these cells functionally connect different brain areas providing feedforward inhibition onto cortical cells.

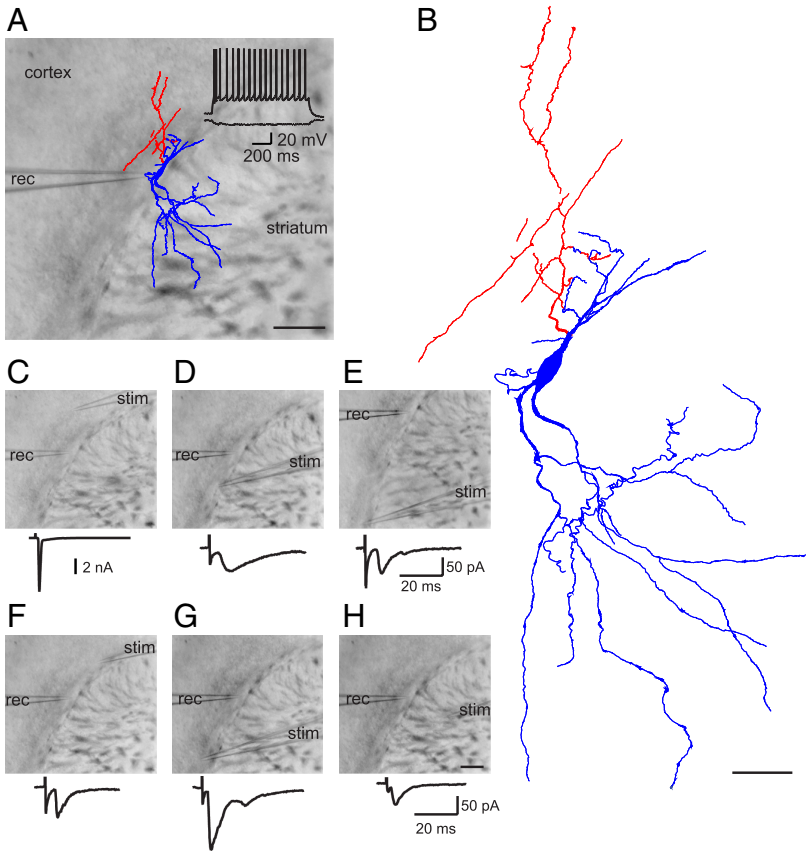

Figure 5. Example of an EGFP-positive neuron in the lateral part of the subcortical white matter connecting different brain areas. ***A***, Reconstruction of a biocytin-filled cell superimposed on the DIC image of the acute slice. The cell body was located in the white matter, dendrites (blue) were arborized in the striatum, and the axon (red) was localized in the white matter and the adjacent cortex. The voltage response of the cell to hyperpolarizing and depolarizing current injection is shown at the top. Scale bar, 200 μm ***B***, Higher magnification of the reconstructed cell. Scale bar, 50 μm. ***C–H***, Images with recording (rec) and stimulation (stim) pipette at different locations. ***C***, A backpropagating action current was elicited upon cortical stimulation. EPSCs were evoked by extracellular stimulation in the white matter (***D–G***) and striatum (***H***). Scale bar: (in ***H***) ***C–H***, 200 μm.

Paired recording allowed us to identify in one cell pair the presynaptic principal cell that was located in layer 6 of the adjacent cortical area. EPSCs could be evoked by extrasynaptic stimulation fairly far away from the postsynaptic WMIC (up to 1 mm). Interestingly, interstitial cells received input not only from the ipsilateral but also the contralateral hemisphere. Previous studies had also shown that interstitial interneurons receive excitatory and inhibitory input (Torres-Reveron and Friedlander, 2007),

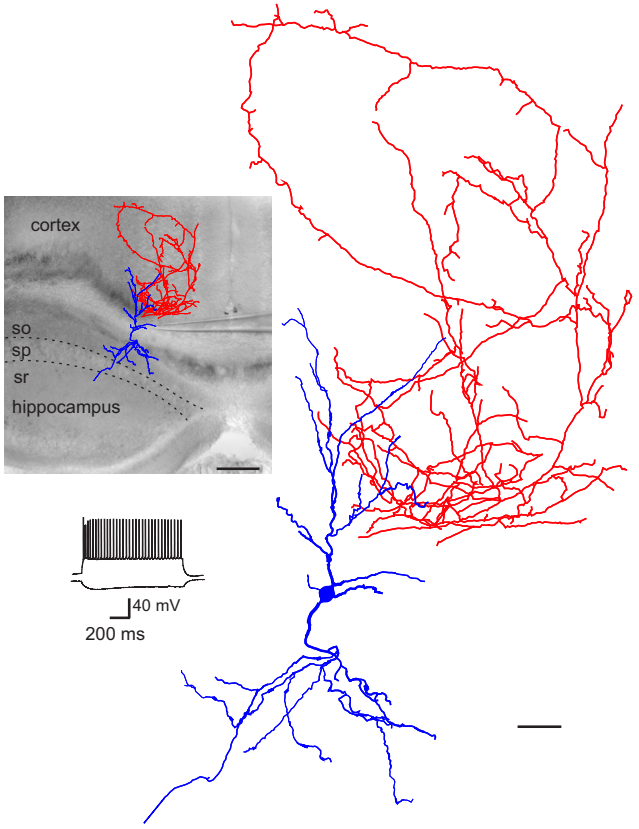

Figure 6. Example of an EGFP-positive neuron in the corpus callosum connecting different brain areas. Reconstruction of a biocytin-filled cell superimposed on the DIC image of the acute slice. The cell body was located in the corpus callosum, dendrites (blue) arborized in the cortex and hippocampus, and the axon (red) was localized in the cortex. Scale bar, 200 μm. The voltage response of the cell to hyperpolarizing and depolarizing current injection is shown below; a higher magnification of the reconstructed WMIC is on the right. Scale bar, 50 μm, so, Stratum oriens; sp, stratum pyramidale; sr, stratum radiatum.

but so far information regarding the output of WMICs onto cortical cells could be inferred only on the basis of reconstructed WMICs and retrograde labeling studies (Meyer et al., 1991; Clancy et al., 2001). In this study we provided the first electrophysiological evidence for the GABAergic phenotype of distinct WMICs by directly demonstrating that EGFP-positive white matter cells inhibited neurons in adjacent cortical areas. The postsynaptic targets were principal neurons and interneurons, but the low number of successful paired recordings (5 of 230) precluded a systematic analysis of the postsynaptic cell type.

EGFP-positive cells received glutamatergic and GABAergic inputs, but 5-HT_3 receptor-mediated spontaneous or evoked currents were absent. 5-HT_3 receptor-mediated currents could readily be evoked in most EGFP-expressing cells by pressure application of serotonin, ruling out EGFP misexpression in WMICs. Although sparse serotonergic innervation of EGFP-positive cells cannot be excluded, a more likely scenario is that 5-HT_3 receptor localization in EGFP-positive cells is not postsynaptic but either extrasynaptic or presynaptic. In fact, in many brain regions 5-HT_3 receptor-bearing neurons do not receive synaptic serotonergic innervation and serotonergic axons often do not form classical synapses (Descarries et al., 1990; Umbriaco et al., 1995), implying volume transmission as the predominant way by which serotonin exerts its function. There is also ample evidence for the existence of presynaptic 5-HT_3 receptors in different brain areas (Nichols and Mollard, 1996; Nayak et al., 1999; Miquel et al., 2002), and functional analyses demonstrated that presynaptic 5-HT_3 receptors can regulate GABA release (Ropert and Guy, 1991; Glaum et al., 1992; Koyama et al., 2000; Katsurabayashi et al., 2003; Turner et al., 2004).

Together with subplate cells, WMICs are among the earliest generated neurons during cortical neurogenesis. The overlapping birth date and location (i.e., below the cortical plate) has led to the widely believed hypothesis that WMICs are remnants of subplate cells (Allendoerfer and Shatz, 1994). However, "early-generated neurons" below the cortical plate are not homogeneous. Subplate cells play a crucial role in the correct formation of thalamocortical innervation during development. In the rodent, most subplate cells are situated in a layer directly below the cortical plate (Allendoerfer and Shatz, 1994) and should be distinguished from "early-generated neurons" in the lower intermediate zone—i.e., the embryonic white matter (Marin-Padilla, 1988)—below the subplate (Van Eden et al., 1989; Del Rio et al., 1992; DeDiego et al., 1994). The latter are GABAergic cells that, after generation in the ganglionic eminences, migrate tangentially in the lower intermediate zone (Van Eden et al., 1989; DeDiego et al., 1994; Tamamaki et al., 1997) and include 5-HT_{3A}-receptor-expressing interneurons born in the caudal ganglionic eminence between embryonic day (E)11.5 and E16.5 (Vucurovic et al., 2010). Most subplate cells apoptose perinatally and postnatally, but some persist into adulthood as a thin layer (layer VIb) between cortex and white matter (Kostovic and Rakic, 1980; Al-Ghoul and Miller, 1989; Chun and Shatz, 1989; Kostovic and Rakic, 1990; Allendoerfer and Shatz, 1994). Differences in perikaryon location, anatomy, and physiology of 5-HT_{3A}-EGFP-positive WMICs and layer VIb neurons (Valverde and Facal-Valverde, 1988; Friauf et al., 1990; Luhmann et al., 2000; Hanganu et al., 2001, 2002, 2009; Torres-Reveron and Friedlander, 2007; Kilb et al., 2008; Zhao et al., 2009) support the notion that in rodents GABAergic WMICs descend from lower intermediate zone GABAergic cells and not from subplate neurons (DeDiego et al., 1994; Tamamaki et al., 1997, 2003a, 2003b; Okhotin and Kalinichenko, 2003).

In summary, we described here 5-HT_{3A} receptor-bearing GABAergic WMICs that resemble cortical interneurons based on morphology, interneuron marker expression, and electrophysiological features. We have provided functional evidence that these defined GABAergic WMICs are functionally integrated into neuronal networks, receiving excitatory and inhibitory inputs and providing feedforward inhibition onto cortical cells.

References

Adrian TE, Allen JM, Bloom SR, Ghatei MA, Rossor MN, Roberts GW, Crow TJ, Tatemoto K, Polak JM (1983) Neuropeptide Y distribution in human brain. Nature 306:584–586.

Al-Ghoul WM, Miller MW (1989) Transient expression of Alz-50 immunoreactivity in developing rat neocortex: a marker for naturally occurring neuronal death? Brain Res 481:361–367.

Allendoerfer KL, Shatz CJ (1994) The subplate, a transient neocortical structure: its role in the development of connections between thalamus and cortex. Annu Rev Neurosci 17:185–218.

Bayraktar T, Staiger JF, Acsady L, Cozzari C, Freund TF, Zilles K (1997) Co localization of vasoactive intestinal polypeptide, gamma-aminobutyric acid and choline acetyltransferase in neocortical interneurons of the adult rat. Brain Res 757:209–217.

Bayraktar T, Welker E, Freund TF, Zilles K, Staiger JF (2000) Neurons immunoreactive for vasoactive intestinal polypeptide in the rat primary somatosensory cortex: morphology and spatial relationship to barrel-related columns. J Comp Neurol 420:291–304.

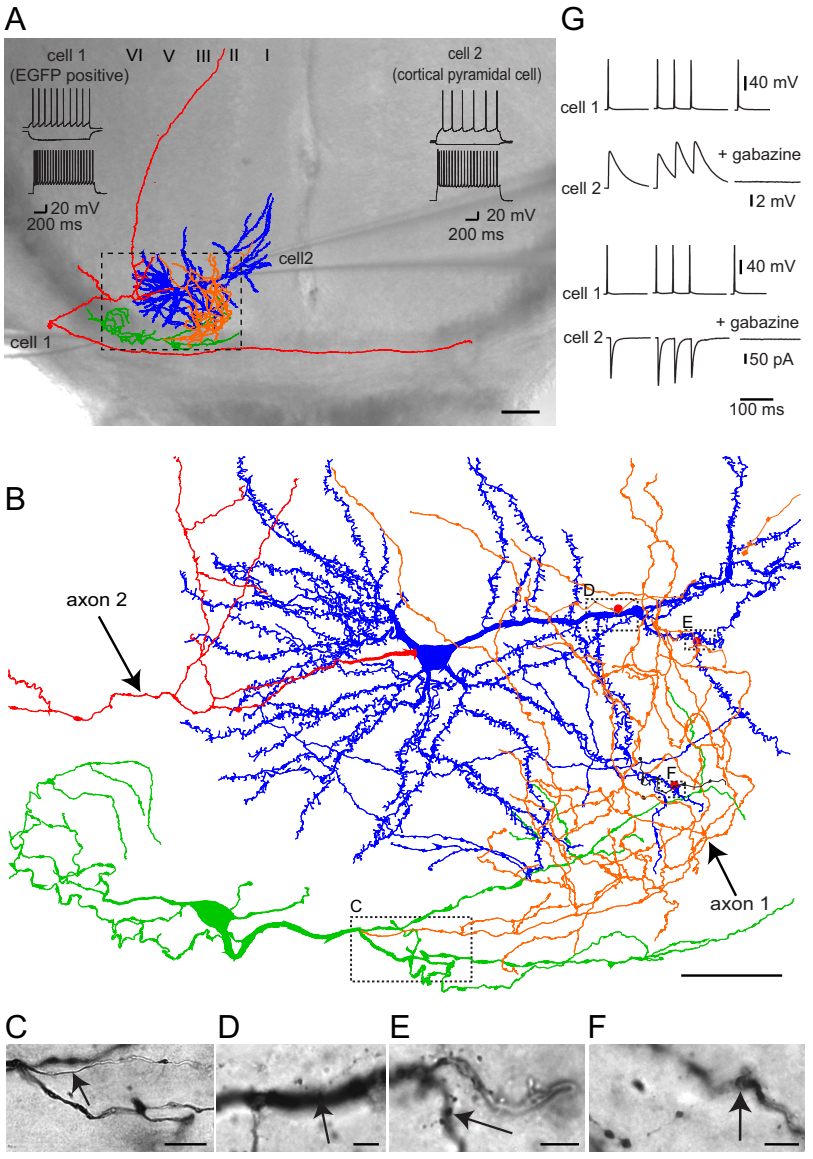

Figure 7. EGFP-positive WMICs inhibit cortical neurons. ***A***, Reconstruction of a biocytin-filled cell pair superimposed on the DIC image of the acute slice. The EGFP-positive WMIC (cell 1) inhibited the postsynaptic cortical spiny pyramidal cell (cell 2). The axon of the pyramidal cell (red) entered the corpus callosum and traveled to the contralateral hemisphere. The axon of the WMIC (orange) entered the cortex where it overlapped with the dendritic arbor of the cortical cell (blue). The WMIC dendritic arbor (green) was located in the corpus callosum. Scale bar, 100 μm. Voltage responses to hyperpolarizing (middle traces), suprathreshold (top traces), and submaximal (bottom traces) current injections are shown at the top of the DIC image. Cell 1 exhibited a nonadapting firing pattern with an initial burst and cell 2 a typical pyramidal cell firing pattern. ***B***, Higher magnification of part of the reconstructed cell pair (stipulated box in ***A***) with red dots indicating where axon boutons of cell 1 were in close proximity to spiny dendrites of cell 2 (putative synapses). Boxes indicate location of bright-field images shown below. Scale bar, 50 μm ***C***, Bright-field image of the biocytin-filled cell with the beginning of the axon (arrow) emerging from a primary dendrite. Scale bar, 10 μm ***D–F***, Bright-field images with putative synapses. Arrows point to WMIC axon boutons in close proximity to pyramidal cell dendrites. Scale bars, 5 μm ***G***, Action potentials in cell 1 elicited IPSPs (top traces) and IPSCs (bottom traces) in cell 2 that showed paired-pulse depression at a frequency of 50 Hz and could be blocked by the $GABA_A$ receptor antagonist gabazine.

Chan-Palay V, Allen YS, Lang W, Haesler U, Polak JM (1985) Cytology and distribution in normal human cerebral cortex of neurons immunoreactive with antisera against neuropeptide Y. J Comp Neurol 238:382–389.

Chun JJ, Shatz CJ (1989) Interstitial cells of the adult neocortical white matter are the remnant of the early generated subplate neuron population. J Comp Neurol 282:555–569.

Clancy B, Silva-Filho M, Friedlander MJ (2001) Structure and projections of white matter neurons in the postnatal rat visual cortex. J Comp Neurol 434:233–252.

DeDiego I, Smith-Fernández A, Fairén A (1994) Cortical cells that migrate beyond area boundaries: characterization of an early neuronal population in the lower intermediate zone of prenatal rats. Eur J Neurosci 6:983–997.

Del Rio JA, Soriano E, Ferrer I (1992) Development of GABA-immunoreactivity in the neocortex of the mouse. J Comp Neurol 326:501–526.

Descarries L, Audet MA, Doucet G, Garcia S, Oleskevich S, Séguéla P, Soghomonian JJ, Watkins KC (1990) Morphology of central serotonin neurons. Brief review of quantified aspects of their distribution and ultrastructural relationships. Ann N Y Acad Sci 600:81–92.

Eastwood SL, Harrison PJ (2005) Interstitial white matter neuron density in the dorsolateral prefrontal cortex and parahippocampal gyrus in schizophrenia. Schizophr Res 79:181–188.

Friauf E, McConnell SK, Shatz CJ (1990) Functional synaptic circuits in the subplate during fetal and early postnatal development of cat visual cortex. J Neurosci 10:2601–2613.

Friedlander MJ, Torres-Reveron J (2009) The changing roles of neurons in the cortical subplate. Front Neuroanat 3:15.

Glaum SR, Brooks PA, Spyer KM, Miller RJ (1992) 5-Hydroxytryptamine-3 receptors modulate synaptic activity in the rat nucleus tractus solitarius in vitro. Brain Res 589:62–68.

Hanganu IL, Kilb W, Luhmann HJ (2001) Spontaneous synaptic activity of subplate neurons in neonatal rat somatosensory cortex. Cereb Cortex 11:400–410.

Hanganu IL, Kilb W, Luhmann HJ (2002) Functional synaptic projections onto subplate neurons in neonatal rat somatosensory cortex. J Neurosci 22:7165–7176.

Hanganu IL, Okabe A, Lessmann V, Luhmann HJ (2009) Cellular mechanisms of subplate-driven and cholinergic input-dependent network activity in the neonatal rat somatosensory cortex. Cereb Cortex 19:89–105.

Higo S, Udaka N, Tamamaki N (2007) Long-range GABAergic projection neurons in the cat neocortex. J Comp Neurol 503:421–431.

Higo S, Akashi K, Sakimura K, Tamamaki N (2009) Subtypes of GABAergic neurons project axons in the neocortex. Front Neuroanat 3:25.

Innis RB, Corrêa FM, Uhl GR, Schneider B, Snyder SH (1979) Cholecystokinin octapeptide-like immunoreactivity: histochemical localization in rat brain. Proc Natl Acad Sci U S A 76:521–525.

Inta D, Alfonso J, von Engelhardt J, Kreuzberg MM, Meyer AH, van Hooft JA, Monyer H (2008) Neurogenesis and widespread forebrain migration of distinct GABAergic neurons from the postnatal subventricular zone. Proc Natl Acad Sci U S A 105:20994–20999.

Katsurabayashi S, Kubota H, Tokutomi N, Akaike N (2003) A distinct distribution of functional presynaptic 5-HT receptor subtypes on GABAergic nerve terminals projecting to single hippocampal CA1 pyramidal neurons. Neuropharmacology 44:1022–1030.

Kawaguchi Y, Kubota Y (1996) Physiological and morphological identification of somatostatin- or vasoactive intestinal polypeptide-containing cells among GABAergic cell subtypes in rat frontal cortex. J Neurosci 16:2701–2715.

Kawaguchi Y, Kubota Y (1997) GABAergic cell subtypes and their synaptic connections in rat frontal cortex. Cereb Cortex 7:476–486.

Kilb W, Hanganu IL, Okabe A, Sava BA, Shimizu-Okabe C, Fukuda A, Luhmann HJ (2008) Glycine receptors mediate excitation of subplate neu-

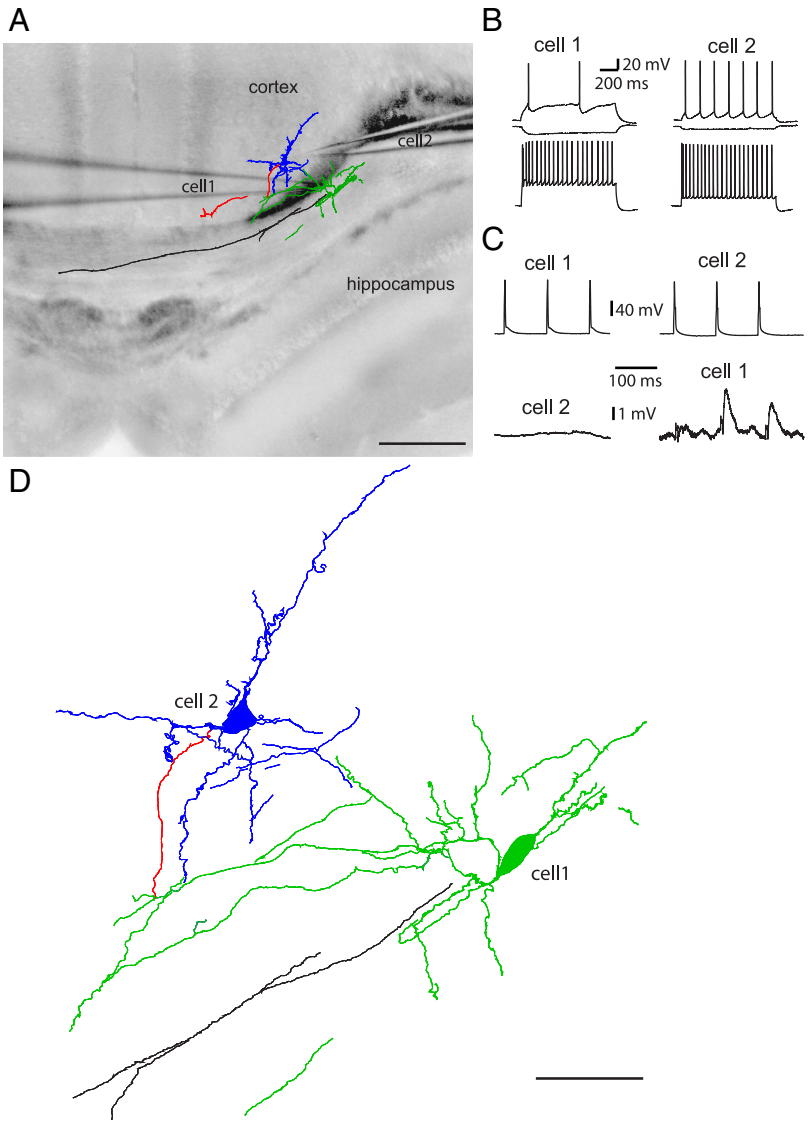

Figure 8. EGFP-positive WMICs are excited by cortical principal cells. ***A***, Reconstruction of a biocytin-filled cell pair superimposed on the DIC image of the acute slice. The EGFP-positive WMIC (cell 1) was excited by the cortical cell (cell 2). Black, WMICs axon; red, cortical cell axon; green, WMICs dendrites; blue, cortical cell dendrites. Scale bar, 200 μm. ***B***, Voltage responses to hyperpolarizing (middle traces), suprathreshold (top traces), and submaximal (bottom traces) current injections. ***C***, Action potentials in cell 1 did not elicit voltage responses in cell 2. In contrast, action potentials in cell 2 elicited facilitating EPSPs in cell 1. ***D***, Higher magnification of part of the reconstructed cell pair. Scale bar, 50 μm.

rons in neonatal rat cerebral cortex. J Neurophysiol 100: 698–707.
Kostovic I, Rakic P (1980) Cytology and time of origin of interstitial neurons in the white matter in infant and adult human and monkey telencephalon. J Neurocytol 9:219–242.
Kostovic I, Rakic P (1990) Developmental history of the transient subplate zone in the visual and somatosensory cortex of the macaque monkey and human brain. J Comp Neurol 297:441–470.
Koyama S, Matsumoto N, Kubo C, Akaike N (2000) Presynaptic 5-HT3 receptor-mediated modulation of synaptic GABA release in the mechanically dissociated rat amygdala neurons. J Physiol 529:373–383.
Loup F, Picard F, Yonekawa Y, Wieser HG, Fritschy JM (2009) Selective changes in GABAA receptor subtypes in white matter neurons of patients with focal epilepsy. Brain 132:2449–2463.
Luhmann HJ, Reiprich RA, Hanganu I, Kilb W (2000) Cellular physiology of the neonatal rat cerebral cortex: intrinsic membrane properties, sodium and calcium currents. J Neurosci Res 62:574–584.
Lund JS, Lund RD, Hendrickson AE, Bunt AH, Fuchs AF (1975) The origin of efferent pathways from the primary visual cortex, area 17, of the macaque monkey as shown by retrograde transport of horseradish peroxidase. J Comp Neurol 164:287–303.
Marin-Padilla M (1988) Early ontogenesis of the human cerebral cortex. In: Cerebral cortex (Peters A, Jones EG, eds), pp xviii, 518. New York: Plenum.
Markram H, Toledo-Rodriguez M, Wang Y, Gupta A, Silberberg G, Wu C (2004) Interneurons of the neocortical inhibitory system. Nat Rev Neurosci 5:793–807.
Meyer G, Gonzalez-Hernandez T, Galindo-Mireles D, Castañeyra-Perdomo A, Ferres-Torres R (1991) The efferent projections of neurons in the white matter of different cortical areas of the adult rat. Anat Embryol (Berl) 184:99–102.
Miquel MC, Emerit MB, Nosjean A, Simon A, Rumajogee P, Brisorgueil MJ, Doucet E, Hamon M, Vergé D (2002) Differential subcellular localization of the 5-HT3-As receptor subunit in the rat central nervous system. Eur J Neurosci 15:449–457.
Mizukawa K, Vincent SR, McGeer PL, McGeer EG (1988) Reduced nicotinamide adenine dinucleotide phosphate (NADPH)-diaphorase-positive neurons in cat cerebral white matter. Brain Res 461:274–281.
Morales M, Bloom FE (1997) The 5-HT3 receptor is present in different subpopulations of GABAergic neurons in the rat telencephalon. J Neurosci 17:3157–3167.
Müller T (1994) Large nerve cells with long axons in the granular layer and white matter of the murine cerebellum. J Anat 184:419–423.
Nayak SV, Rondé P, Spier AD, Lummis SC, Nichols RA (1999) Calcium changes induced by presynaptic 5-hydroxytryptamine-3 serotonin receptors on isolated terminals from various regions of the rat brain. Neuroscience 91:107–117.
Neuburger K (1922) Zur histopathologie der multiplen sklerose im kindesalter. Z Neurol 76:384–414.
Nichols RA, Mollard P (1996) Direct observation of serotonin 5-HT3 receptor-induced increases in calcium levels in individual brain nerve terminals. J Neurochem 67:581–592.
Okhotin VE, Kalinichenko SG (2003) Subcortical white matter interstitial cells: their connections, neurochemical specialization, and role in the histogenesis of the cortex. Neurosci Behav Physiol 33:177– 194.
Raghanti MA, Spocter MA, Stimpson CD, Erwin JM, Bonar CJ, Allman JM, Hof PR, Sherwood CC (2009) Species-specific distributions of tyrosine hydroxylase-immunoreactive neurons in the prefrontal cortex of anthropoid primates. Neuroscience 158:1551–1559.
Ramon y Cajal S (1911) Histologie du systeme nerveux de l'homme et des vertebres. Paris: Maloine.
Ropert N, Guy N (1991) Serotonin facilitates GABAergic transmission in the CA1 region of rat hippocampus in vitro. J Physiol 441:121–136.
Sandell JH (1986) NADPH diaphorase histochemistry in the macaque striate cortex. J Comp Neurol 251:388–397.
Schmechel DE, Vickrey BG, Fitzpatrick D, Elde RP (1984) GABAergic neurons of mammalian cerebral cortex: widespread subclass defined by somatostatin content. Neurosci Lett 47:227–232.
Shering AF, Lowenstein PR (1994) Neocortex provides direct synaptic input to interstitial neurons of the intermediate zone of kittens and white matter of cats: a light and electron microscopic study. J Comp Neurol 347:433–443.
Shults CW, Quirion R, Chronwall B, Chase TN, O'Donohue TL (1984) A comparison of the anatomical distribution of substance P and sub-

stance P receptors in the rat central nervous system. Peptides 5:1097–1128.

Smiley JF, Levey AI, Mesulam MM (1999) M_2 muscarinic receptor immunolocalization in cholinergic cells of the monkey basal forebrain and striatum. Neuroscience 90:803–814.

Somogyi P, Hodgson AJ, Smith AD, Nunzi MG, Gorio A, Wu JY (1984) Different populations of GABAergic neurons in the visual cortex and hippocampus of cat contain somatostatin- or cholecystokinin-immunoreactive material. J Neurosci 4:2590–2603.

Suárez-Solá ML, González-Delgado FJ, Pueyo-Morlans M, Medina-Bolívar OC, Hernández-Acosta NC, González-Gómez M, Meyer G (2009) Neurons in the white matter of the adult human neocortex. Front Neuroanat 3:7.

Tamamaki N, Tomioka R (2010) Long-range GABAergic connections distributed throughout the neocortex and their possible function. Front Neurosci 4:202.

Tamamaki N, Fujimori KE, Takauji R (1997) Origin and route of tangentially migrating neurons in the developing neocortical intermediate zone. J Neurosci 17:8313–8323.

Tamamaki N, Fujimori K, Nojyo Y, Kaneko T, Takauji R (2003a) Evidence that Sema3A and Sema3F regulate the migration of GABAergic neurons in the developing neocortex. J Comp Neurol 455:238–248.

Tamamaki N, Yanagawa Y, Tomioka R, Miyazaki J, Obata K, Kaneko T (2003b) Green fluorescent protein expression and colocalization with calretinin, parvalbumin, and somatostatin in the GAD67-GFP knock-in mouse. J Comp Neurol 467:60–79.

Tao Z, Van Gool D, Lammens M, Dom R (1999) NADPH-diaphorase-containing neurons in cortex, subcortical white matter and neostriatum are selectively spared in Alzheimer's disease. Dement Geriatr Cogn Disord 10:460–468.

Tecott LH, Maricq AV, Julius D (1993) Nervous system distribution of the serotonin 5-HT3 receptor mRNA. Proc Natl Acad Sci U S A 90:1430–1434.

Tomioka R, Rockland KS (2007) Long-distance corticocortical GABAergic neurons in the adult monkey white and gray matter. J Comp Neurol 505:526–538.

Tomioka R, Okamoto K, Furuta T, Fujiyama F, Iwasato T, Yanagawa Y, Obata K, Kaneko T, Tamamaki N (2005) Demonstration of long-range GABAergic connections distributed throughout the mouse neocortex. Eur J Neurosci 21:1587–1600.

Torres-Reveron J, Friedlander MJ (2007) Properties of persistent postnatal cortical subplate neurons. J Neurosci 27:9962–9974.

Turner TJ, Mokler DJ, Luebke JI (2004) Calcium influx through presynaptic 5-HT3 receptors facilitates GABA release in the hippocampus: in vitro slice and synaptosome studies. Neuroscience 129:703–718.

Umbriaco D, Garcia S, Beaulieu C, Descarries L (1995) Relational features of acetylcholine, noradrenaline, serotonin and GABA axon terminals in the stratum radiatum of adult rat hippocampus (CA1). Hippocampus 5:605–620.

Valverde F, Facal-Valverde MV (1988) Postnatal development of interstitial (subplate) cells in the white matter of the temporal cortex of kittens: a correlated Golgi and electron microscopic study. J Comp Neurol 269:168–192.

Van Eden CG, Mrzljak L, Voorn P, Uylings HB (1989) Prenatal development of GABA-ergic neurons in the neocortex of the rat. J Comp Neurol 289:213–227.

von Engelhardt J, Eliava M, Meyer AH, Rozov A, Monyer H (2007) Functional characterization of intrinsic cholinergic interneurons in the cortex. J Neurosci 27:5633–5642.

Vucurovic K, Gallopin T, Ferezou I, Rancillac A, Chameau P, van Hooft JA, Geoffroy H, Monyer H, Rossier J, Vitalis T (2010) Serotonin 3A receptor subtype as an early and protracted marker of cortical interneuron subpopulations. Cereb Cortex 20:2333–2347.

Yan YH, Winarto A, Mansjoer I, Hendrickson A (1996) Parvalbumin, calbindin, and calretinin mark distinct pathways during development of monkey dorsal lateral geniculate nucleus. J Neurobiol 31:189–209.

Zhao C, Kao JP, Kanold PO (2009) Functional excitatory microcircuits in neonatal cortex connect thalamus and layer 4. J Neurosci 29:15479–15488.